MODELLING THE HYDROTHERMODYNAMICS OF THE SURFACE LAYER OF A STRATIFIED TROPICAL SUBTROPICAL OCEAN

C. A. A. Carbonel H.[a], and A. C. Galeão[b]

[a] Laboratório Nacional de Computação Científica
Departamento de Mecânica Computacional
Av. Getúlio Vargas 333, Quitandinha
Petrópolis, Rio de Janeiro, Brasil carbonel@lncc.br

[b] Laboratório Nacional de Computação Científica
Departamento de Mecânica Computacional
Av. Getúlio Vargas 333, Quitandinha
Petrópolis, Rio de Janeiro, Brasil
acng@lncc.br

ABSTRACT

In the present paper a two-layer model is developed for the non-permanent hydrothermodynamics of a tropical subtropical coastal ocean. The model includes the equations of motion, continuity and heat. The equations apply only to the thin and warm oceanic surface layer. The deep layer is stipulated to be motionless, arbitrarily deep and separated from the upper layer by a density discontinuity. Cold deep water is carried across the interface from the lower into the upper layer; it is warmed up there by the net energy input from the atmosphere into the ocean The non-uniform sea surface wind stress and heat at the surface are the main forcing functions of the model. A numerical finite element method is proposed to approximate the hydrothermodynamic problem. The model uses simple linear spatial and temporal continuous polynomial and a stabilizing Petrov-Galerkin operator to improve the classical finite element Galerkin method. The hydrothermodynamic response is obtained for the eastern pacific boundary in the southern hemisphere. Monthly climatological data are used to determine the wind and heat fluxes forcings of the model. The main features of the observed Sea Surface Temperature (SST) pattern are successfully simulated by the model. In particular the predicted : upwelling along the coastal boundary; warm water intrusion in offshore side and signals of countercurrents are in a quite good agreement with observations.

Keywords: Hydrothermodynamics, Ocean models, Eastern ocean boundaries, Finite elements, Petrov-Galerkin formulation.

NOMENCLATURE

b	$b = Tc_0 / T^u$, m/s
c	wave celerity, m/s
c_0	referential wave celerity, m/s
C_H, C_e	dimensionless parameters
c_{pa}	specific heat of the air, J/(kg°C)
c_p	specific heat of the surface water, J/(kg°C)
d	$d=2c$ m/s
f	Coriolis parameter, sec^{-1}
H`	initial upper layer thickness, m
H_e	depth scale of the entrainment process, m
h	upper layer thickness, m
L	latent heat of evaporation J/kg
N	number of finite element sub-domains
P^k	set of piecewise polynomials of degree $\leq k$
Q	net heat flux across the surface, Watt/m^2
Q_I	heat flux across the interface, Watt/m2
Q_s	net short wave radiation , Watt/m^2
Q_{lw}	outgoing longwave radiation, Watt/m^2
Q_h	sensible heat flux, Watt/m^2
Q_e	latent heat flux, Watt/m^2
q	saturation specific humidity
R^2	the space of (x,y) points
R	*Riemann* invariant
S_n	space-time finite element "slab"
T	sea surface temperature (SST), °C
T^u	referential initial upper layer temperature, °C
T^l	lower layer temperature, °C
t_e	time scales of the entrainment process, sec
u, v	velocity components in the upper layer, m/s
u_n	velocity normal to the open boundary, m/s
U_n^h	set of admissible trial functions
$\hat{U}_n^h$	finite element subspace of weighting functions
V^h	trial function
$\hat{V}^h$	weighting function
w_e	entrainment velocity, m/s
	divergence velocity, m/s
x_n	axis normal to the open boundary
x,y	cartesian coordinates

Greek symbols

	coefficient of thermal expansion, °C^{-1}
$_L$	land type boundary
$_O$	open ocean boundary.
$_{h,\,t}$	space time partition space domain
Ω_e	finite element sub-domain
Ω	space domain
$\frac{e}{}$	boundary sub-domain
$_e$	matrix of intrinsic time scale
ϑ	eddy viscosity, m^2/s
ϑ_T	thermal diffusivity, m^2/s
	the empty set
$_{air}$	density of air, kg/m^3
$_u$	density of the upper layer, kg/m^3
$_l$	density of the lower layer, kg/m^3
$_{x,\,y}$	wind stress components, N/m^2

INTRODUCTION

The most familiar characteristic of eastern boundary currents (EBCs), is the importance of equatorward surface currents and coastal upwelling resulting from a predominantly equatorward wind stress. The EBCs feature large stocks of small pelagic fish, which provide about one third of the world's total catch of fish. Also the EBCs have some commonality in their physical structure and the

mechanisms that force their oceanographic character (Parrish et al., 1983; Lluch-Belda et al., 1992). The existence of undercurrents is a dynamical feature that increases the complexity of the eastern boundary ocean dynamics.

In order to interpret this dynamics, and provide a dynamical basis for its prediction, it is necessary to consider the circulation in a large extended area of the eastern oceans. An important issue is to develop a hydrodynamic model which shows that upwelling, the horizontal circulation and sea surface temperature (SST) fields are associated phenomena. A first contribution attempt to explain the circulation in the eastern tropical oceans was provided by Yoshida (1967). He proposed a theoretical permanent two layer model, that qualitatively reproduces the topography of sea surface, thermocline, and poleward coastal underrcurrents which are dynamically related to upwelling.

Other numerical studies in the 70's were developed for the eastern pacific ocean, (e.g. Hulburt, 1974; O'Brien et. Al. 1979; Preller and O'Brien, 1980), using the finite difference method (FDM). In these studies, oriented to the upwelling response, the influence of the coastline geometry and bottom topography were focused. Despite remarkable achievements gained with the finite element method (FEM) in simulating coastal and tidal dynamics, ocean general circulation models (OGCMs) used in climatic studies still almost exclusively rely on the FDM. The only exception is the spectral element ocean model (SEOM) (Iskandarani et al., 1995). One of the main difficulties using FEM is the unphysical wave scattering due to changes in grid spacing. For classical steady state engineering problems or even for ocean circulation problems at relatively short integration time (tidal and coastal models), this drawback could be of minor importance.

Nevertheless, for large scale ocean circulation modelling it might become of crucial importance.

In the context of FEM, those numerical spurious oscillations could be effectively supressed using a consistent variational Petrov-Galerkin (PG) formulation to improve the classical finite element Galerkin approximation. This approach gives rise to the well known "Streamline Upwind Petrov-Galerkin (SUPG) method, and other related shock-capturing operators initially proposed for advection-difusion and compressible flow problems (e.g. Brooks and Hughes, 1982; Shakib, 1988; Almeida, Galeão, Silva, 1996). Other PG formulations using a symmetric form of the shallow water wave equations were reported in last years (e.g. Bova and Carey,1995; Carbonel, Galeão and Loula, 2000). For hydrodynamic baroclinic circulation, a similar approach was recently presented (Carbonel and Galeão 2004) focusing the wind-driven dynamic response in open and limited areas.

Here, a 1 ½ layer finite element model (called in this way by the fact that the lower layer exists but without motion) of limited area domain is proposed to describe the upper layer dynamics in the eastern boundary pacific ocean. This model includes the hydrodynamic and thermodynamic of the surface ocean layer forced by fields of wind and heat fluxes. A space-time PG formulation is used to guarantee the required accuracy and stability for the derived discrete model.

As it will be shown, only the spatial region of interest needs to be discretized, precluding the simulation of all the pacific ocean as done in many other related works. This strategy allows the use of a well refined mesh to accurately capture the main features of the observed SST pattern. Since the eastern pacific coastal current system have a complex vertical structure and current configuration, the present paper is a first step in the study of the eastern pacific ocean. Our main purpose here is to prove the ability of the proposed model to predict the surface tendency response when subjected to mean forcing functions. Also, it is very important to determine in what extent the observed features of the SST depend on the mentioned forcings.

The pacific coast is a typical upwelling region due to the permanent favourable winds. During the summer months the coastal upwelling continues, but warming waters from the north invader the region mainly in the offshore side. Figure 1a shows the mean SST for February in the eastern pacific ocean (Da Silva et.al, 1994). It is observed that warmer water occupies an important part of the region. The contour of 23°C describes a warm plume that reaches the 20°S. Colder water are observed in the south side of the studied area, and along the coast between the 10°S to 17°S. The simultaneous existence of colder waters near the coast and a southward warmer intrusion offshore, configures strong SST gradients which are a challenge for modelling coastal ocean processes. Therefore, in this paper we focused the modelling objectives into the evaluation of the hydro-thermodynamics for the summer month of February.

It is known that the dynamics of both wind stress and SST tend to be divided into three regions (Figure 1b), with a transition zone that varies in extent through time, and whose dynamic alternately changes from one to the other adjacent zone. The north and south sectors have negative anomalies of SST, whereas central sector has positive anomalies: a common trend that occurs also in the California current system (Mendelshon and Schwing, 2002).

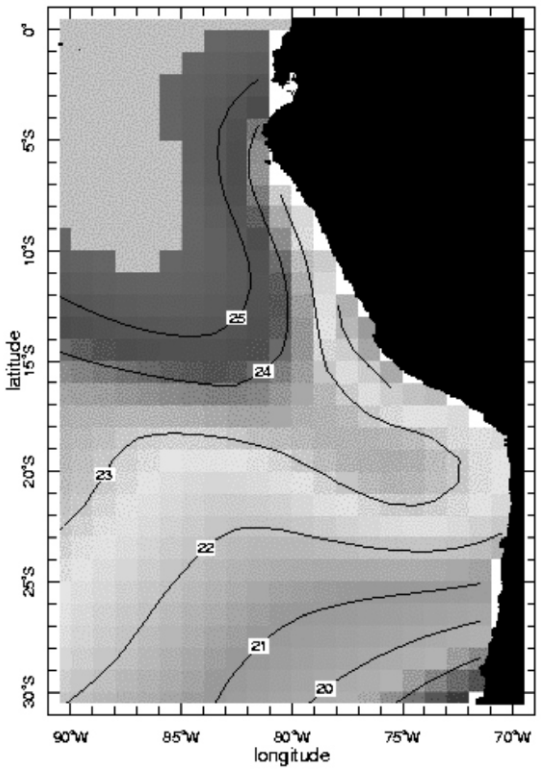

Figure 1a. The mean SST(°C) for February in the easternpacific ocean (from Da Silva et.al, 1994).

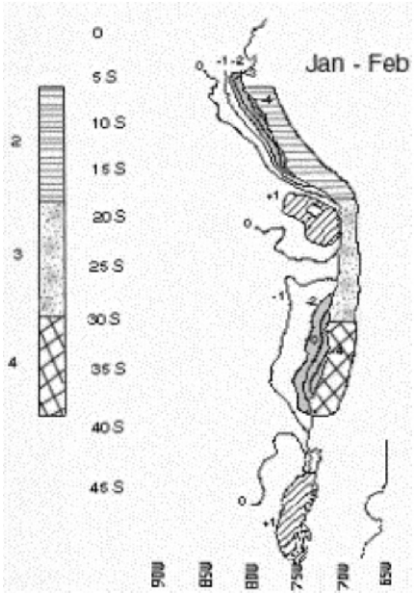

Figure 1b. The SST anomalies corresponding to January, February and the sectors 2, 3 and 4 along the Peru Chile coast (from Mendelshon and Schwing, 2002).

THE OCEAN MODEL

The governing equations

We use cartesian coordinates $(x,y) \in R^2$ oriented positively to the East and North respectively. A coastal ocean is defined in a domain $\Omega \subset R^2$. We consider land type boundary Γ_L and an ocean type boundary Γ_O, such that Γ_O and Γ_L .

Two layers are considered to describe the vertical structure (Figure 2). The upper layer of density ρ^u and thickness h, and an inert lower layer ρ^l where it is assumed that the horizontal pressure gradient is zero. In that way the faster barotropic mode is eliminated and just the first internal baroclinic mode is considered. The thermal structure is defined by the instant upper layer temperature T, and the lower layer temperature T^l.

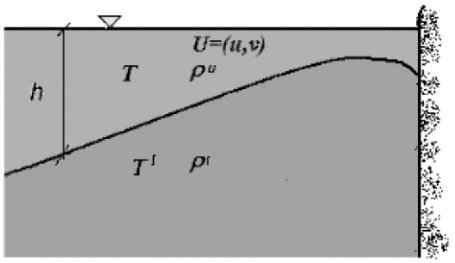

Figure 2. The vertical structure of the two layers ocean system

As a constitutive state equation we assume the *ansatz*

$$^{u} \quad ^{l}[1 \quad (T \quad T^{l})] \tag{1}$$

where T is the actual temperature and the thermal expansion coefficient. The influence of the salinity is not included, but there is no loss of generality, since an apparent temperature could be estimated modifying the constant , to include the salinity concentration effect (Hantel, 1971; Fofonoff, 1962).

For convenience, we define the variables

$$d \quad 2c \quad c \quad \sqrt{g \quad h} \quad b \quad \frac{c^0 T}{T^u} \tag{2}$$

having the dimension of velocity. The parameter g represent the gravity acceleration, $= (T\text{-}T^l)$. and $c^0 \quad \sqrt{g \quad (T^u \quad T^l)H}$ is a referential celerity for the initial upper layer thickness H. T^u is the referential initial temperature in this layer.

Introducing a column array vector of unknown variables $V=(u,v,d,b)^T$, where u, v are the velocity components in the upper layer, the governing system of equations can be written as:

$$\frac{V}{t} \quad \underline{A}\frac{V}{x} \quad \underline{B}\frac{V}{y} \quad \underline{C}V \quad \underline{D}\left(\frac{^2V}{x^2} \quad \frac{^2V}{y^2}\right) \quad F \quad 0 \tag{3}$$

$$\underline{A}= \begin{matrix} u & 0 & c & s \\ 0 & u & 0 & 0 \\ c & 0 & u & 0 \\ 0 & 0 & 0 & u \end{matrix}, \quad \underline{B}= \begin{matrix} v & 0 & 0 & 0 \\ 0 & v & c & s \\ 0 & c & v & 0 \\ 0 & 0 & 0 & v \end{matrix},$$

$$\underline{C}= \begin{matrix} 0 & f & 0 & 0 \\ f & 0 & 0 & 0 \\ 0 & 0 & 0 & 0 \\ 0 & 0 & 0 & 0 \end{matrix}, \quad \underline{D} = \begin{matrix} 0 & 0 & 0 & 0 \\ 0 & & 0 & 0 \\ 0 & 0 & 0 & 0 \\ 0 & 0 & 0 & \end{matrix}_T,$$

$$F= \begin{matrix} -\tau_x / \rho^u h \\ -\tau_y / \rho^u h \\ -w_e g\sigma / c \\ (Q_I \quad Q)/h \end{matrix}, \quad V= \begin{matrix} u \\ v \\ d \\ b \end{matrix}$$

The entrainment velocity w_e, is assumed to be $w_e \quad (H_e \quad h)^2 / t_e H_e$, where H_e and t_e represent respectively the depth and time scales of the entrainment process (see McCreary and Kundu, 1988). The wind stress components are represented by $_x$, $_y$, and f is the Coriolis parameter that depends on the geographical coordinates. The eddy viscosity is represented by ϑ and ϑ_T is the thermal diffusivity. The function $s \quad gh \quad T^u / 2 \quad c^0$; $/(\quad)$; $\mu = \rho^u / \rho^l$; $= 1 - \mu$. At the free surface the heat source is equal to $Q/\rho^u c_p$ (Q defined in Eq. 4). In the interface $Q_I \quad k_I (T \quad T^l)/h$ represent the gain or loss of heat across this interface, depending on the dynamical convergence or divergence of the flows w in the upper layer, and on the parameter $k_I \quad H$ (Carbonel, 2003).

The thermodynamic part of the model is driven by the surface heat flux Q which is defined as

$$Q = Q_s - Q_{lw} - Q_e - Q_h \tag{4}$$

where Q_s is the net short wave radiation, Q_{lw} the resultant outgoing longwave radiation, Q_h $_{air}c_{pa}C_H(T$ $T_{air})|W|$ the sensible heat, and Q_e $_{air}C_eL(q$ $q_{air})|W|$ is the latent heat. In these relations $_{air}$ is the air density; L is the latent heat of evaporation, |W| the wind velocity magnitude, the parameter c_{pa} is the specific heat of the air, C_H, C_e are the Stanton and Dalton dimensionless parameter, and q, q_{air} are the saturation specific humidity of the sea surface and air respectively.

On land type boundaries, we prescribe the non-slip conditions

$$u \quad v \quad 0 \tag{5}$$

and natural boundary conditions are assumed for the upper thickness h and also for the temperature T.

For the open ocean boundary we prescribe a weakly reflective boundary condition presented according to the characteristic method, in an axis (x_n) normal to the open boundary. Along the characteristics $dx_n/dt = u_n \pm c$ it is assumed that the *Riemann* invariant $R^{\pm} = u_n \pm d$ satisfy:

$$\frac{DR}{Dt} \quad 0 \tag{6}$$

where u_n represents the velocity component normal to the boundary. The weakly reflective conditions on the open boundary are defined by the in-going characteristic of the presented equations. (See Carbonel(2003) where the advantages of this kind of open boundaries modelling coastal upwelling were recently reported).

For the temperature at the open boundaries natural condition are used.

Finally an appropriate initial state should be assumed in the domain Ω and at the boundary Γ:

$$u = u^o,\ v = v^o,\ h = h^o,\ T = T^o \ \text{ at } \ t = 0 \tag{7}$$

where u^o, v^o, h^o and T^o represent the initial velocity components, the thickness and the temperature respectively.

Space time Petrov-Galerkin method (STPG)

To approximate the ocean problem previously presented we define a space-time finite element partition $^{h,\ t}$, in which the time interval is partitioned into subintervals

$$I_n = t_{n+1} - t_n = \quad t, \ \ t \in [0, \mathfrak{I}] \tag{8}$$

where t_n, t_{n+1} belong to an ordered partition of time levels $0 = t_0 < ....t_n < t_{n+1} .... < t_F = \mathfrak{I}$.

For each n the space domain Ω is partitioned in sub-domains Ω_e with boundary Γ_e, such that

$$i \qquad j \qquad \text{for } i \neq j;\ \ i,j = 1,...N \tag{9a}$$

$$\qquad N \qquad\qquad\qquad (9b)$$

$$e \ 1 \qquad e$$

As a result, for each $n=1,2...$ the space-time domain of interest is the slab S_n I_n with boundary $_n$ I_n; the lateral surface of this "slab".

Under the above definitions we will assume that the finite element subspace of weighting functions is the set of continuous piecewise polynomials $\hat{V}^h$ in S_n, i.e.

$$\hat{U}^h_n \qquad \hat{V}^h; \hat{V}^h \quad C^0\ S_n \quad ^4;$$

$$\hat{V}^h\big|_{\Omega^e} \quad P^k\ \Omega_e \quad ^4; \hat{V}^h\big|_{\Gamma_n} \quad 0 \tag{10}$$

Note that the previous definition implies that in the spatial domain each component of the vector $\hat{V}^h$ has C^o continuity; its restriction to a particular finite element $_e$ being a polynomial of degree less than or equal to k. Across the slab interfaces those components may be discontinuous. In this work, a continuous and linear interpolation in space and time will be adoptted.

Now let us introduce a vector $\overline{V}^h$ of prescribed boundary conditions on Γ_n. As a consequence, the set U^h_n of admissible trial functions will be:

$$U^h_n \qquad V^h; V^h \quad C^0\ S_n \quad ^4;$$

$$V^h\big|_{\Omega_e} \quad P^k\ \Omega_e \quad ^4; V^h\big|_{\Gamma_n} \quad \overline{V}^h \tag{11}$$

For a general trial function V^h, the residual vector of the equation system (3) reads,

$$R^h \quad \underline{I}\frac{V^h}{t} \quad \underline{A}(V^h)\frac{V^h}{x} \quad \underline{B}(V^h)\frac{V^h}{y}$$

$$\underline{C}(V^h) \quad \underline{D}\left(\frac{^2V^h}{x^2} \quad \frac{^2V^h}{y^2}\right) \quad F \tag{12}$$

Then, we say that the space-time Petrov-Galerkin approximate solution for the hydro-thermodynamic problem is the vector $V^h \in U^h_n$, which satisfies $\hat{V}^h$ $\hat{U}^h_n$ the variational equation:

$$\hat{V}^h R^h d \quad dt \qquad ^N \quad \overline{\quad}_e G^h R^h d \quad dt \quad 0 \tag{13}$$

$$S_n \qquad\qquad e\ 1\ S^e_n$$

where

$$G^h \quad \underline{I}\frac{\hat{V}^h}{t} \quad \underline{A}(V^h)\frac{\hat{V}^h}{x} \quad \underline{B}(V^h)\frac{\hat{V}^h}{y} \tag{14}$$

in a space-time operator, and

$$\overline{\Psi}_e \qquad ^3 \qquad _k e_k e_k^T \tag{15}$$

$$k\ 1$$

is the matrix of stabilizing free parameters. A possible choice for these parameters could be achieved assuming:

$$_k = 1/\sqrt{\ }_k \tag{16}$$

where $_k$ are the eigenvalues of the matrix

$$[(1/\Delta t)^2 \underline{I} + (1/l_x^2)\,\underline{A}^2 + (1/l_y^2)\,\underline{B}^2]^{-1/2} \tag{17}$$

e_k are the associated eigenvectors (see Shakib, 1988; Bova and Carey, 1995; Ribeiro e Galeão, 1996). The parameters l_x, l_y are the characteristics lengths of the finite element.

The algebraic equation system resulting from the PG weighting residual equation (11) will be solved using the direct method of Gauss.

THE SST RESPONSE IN THE EASTERN BOUNDARY PACIFIC OCEAN

For modelling purposes, the studied area extends: in the north-south direction from the equator to the 30°S; and in the east-west direction from the 70° W to 90° W (Figure 3).

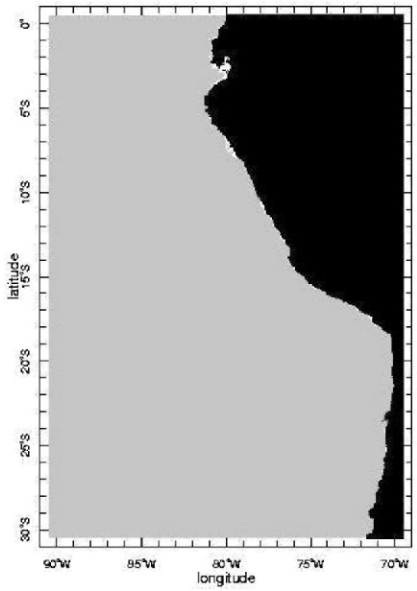

Figure 3. The eastern pacific ocean

There are diverse coastal irregularities, but for our schematic model we only consider the irregularities located at 5°S and at 19°S. The other coastal irregularities, such as the Guayaquil Bay (3°S), and the coastline change located at the Paracas peninsula (14°S), could be added in a next study focusing the detailed role of the indicated coastal configurations in the regional pattern.

The model coastline is a simple schematized configuration of the pacific coast from de 30°S to 0°S, described by straight lines connecting 4 points from south to north 70°W, 30°S; 70°W, 18.6°S; 81°W, 6°S; 81°W, 0°S. The discretized domain corresponds to 1810 nodes and 3419 triangular elements (Figure 4).

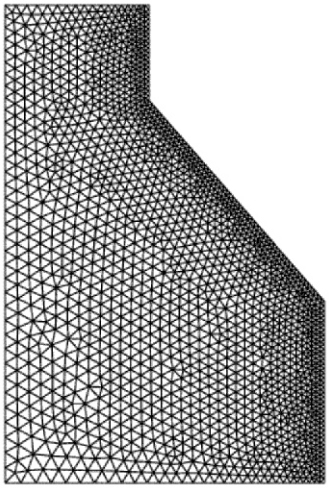

Figure 4. Finite element mesh of the schematised eastern pacific coastal ocean

A finer unstructured finite element mesh is employed near the coastline, which becomes coarser near the offshore region. The smaller sides of the elements along the coastline are of 0.3° , whereas in the left outer boundary the side elements are up to 0.9°.

The numerical experiment performed to evaluate the coastal ocean dynamics assumes that the fluid in the layers are initially at rest; and the following set of parameters is used: The time step is $t = 10800$sec . The densities of the upper and lower layer are ρ^u=1023 kg m^{-3} and ρ^l=1026.5 kgm^{-3}, ρ_{air}=1.175 kg m^{-3}. The initial upper layer thickness is H=50 m. The entrainment depth H_e=30m and the entrainment time scale t_e =0.5 days. The initial upper temperature T^u =26°C, and the lower layer temperature is T^l =15° C. The thermal expansion coefficient is =0.0003 °C^{-1} .

In this experiment, the forcing functions of the model are the February monthly mean fields for the wind stress, net incident heat flux ($Q_n = Q_s - Q_{lw}$), the air temperature T_{air}, and the specific humidity q_{air}. These forcings are extracted from the Atlas of Da Silva et. al. (1994). It is necessary to remark, that in the evaluation of the surface heat flux Q (Eq. 4), the contributions Q_e and Q_h, are obtained using the water temperature T from the model, instead of the observed SST. Other data are: the latent heat of evaporation $L = 2.44 \times 10^6$ J/kg, the parameters C_H, C_e which are equal to 0.0013, and the specific heat of the air c_{pa} = 1004 J/kg. The saturation specific humidity q is evaluated in terms of the saturation vapour pressure (see Rosenfeld et. al. 1994).

The fields τ_x, τ_y, Q_s, Q_{lw} T_{air}, q_{air} were obtained by interpolation of the original data for each node of the mesh. The wind stress and the net heat flux forcing fields during February are presented in Figures 5a and 5b respectively. The wind field shows that the stronger wind stress is located offshore. Nevertheless, strong winds also occur near the coast between the 28°S to 30°S. The net heat flux Q_n shows maximal values along the slanted coastline (~ from 5 to 19° S), which is precisely the same region where the upwelling is more significative. The forcing functions were applied impulsively at t = 0, (the undisturbed rest state), and maintained constant during all the calculation period of 1 month.

The Figure 6 shows the currents and SST fields calculated by the model for that month. The resulting pattern of the temperature contours is very similar to the observed one (see Figure 1a). The numerical solution shows colder waters along the coastline between the 6°S to 19°S and from the 25°S to the south. The coastal upwelling is responsible for the lower SST along the coastal boundary, but the colder waters in the southern offshore side is not of coastal upwelling origin. It could be a consequence of the heat exchange fluxes between the atmosphere and the ocean.

The calculated SST contour of 23°C clearly describes the warm water intrusion observed in the data. The temperature contours show that the warm water intrusion reaches almost all the coast around the 20°S, leading to a reduction of the colder pattern in this sector (between the 19°S to 25°S). This fact could be one of the possible factors which induces the positive anomalies in that region, as reported by Mendelshon and Schwing (2002). The occurrence of warmer temperatures in this sector could be explained by the moderate winds stress dynamic effects in that region, combined with the coastline

changes, that contribute to the increase of the convergence pattern for northward water flow which, on the other hand, is intensively forced by strong N-S wind velocities observed around the 25°S to 30°S near the coast (see Figure 5a).

The calculated current velocity field pattern shows stronger currents in the northern side and a coastal jet alongshore. In the offshore side a weak component to the south is observed in the current field, indicating that a superficial countercurrent is formed. In the real world, these currents are intense. The unrealistic cooling (due to hydrodynamic divergence) in the northern side (0°S to 6°S) is not observed in the original data. Since, in front of the Guayaquil bay (from 81°W to the east) the winds are eastward, the simplified straight coastline representation does not allow the capturing of the real wind stress effects.

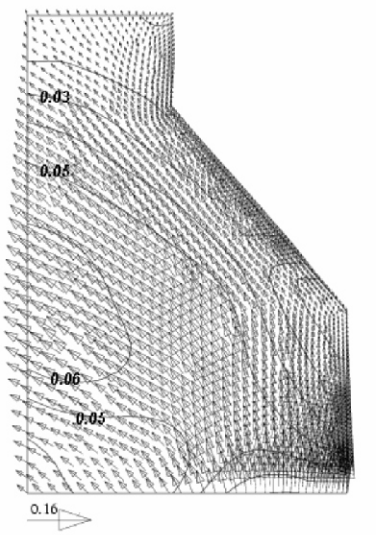

Figure 5a. The Wind Stress field forcing (extracted from Da Silva, 1994). The contours of wind stress magnitude is 0.01Nm^{-2}.

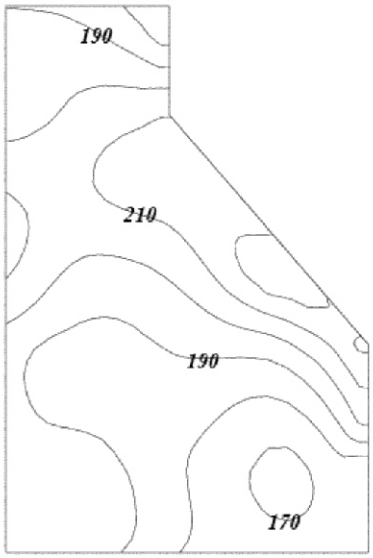

Figure 5b. The net heat flux Q_n (Wm^{-2}) forcing (extracted from Da Silva ,1994).Contours of heat each 10 Wm^{-2}.

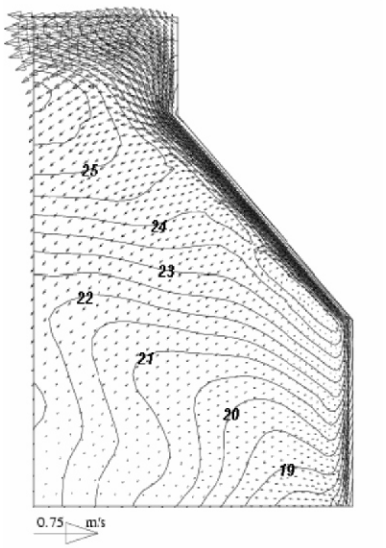

Figure 6. Calculated SST(ºC) and Velocity (ms^{-1}) for February.

SUMMARY AND CONCLUSIONS

A model for the surface layer of stratified waters in the tropical subtropical ocean is presented, taking into account the wind-driven hydro-thermodynamics equations of momentum, continuity and heat transfer. The model considers the essential processes of a gravity reduced dynamics, with an active upper layer and a inert lower layer. The forcing terms include the wind field and the heat fluxes extracted from reported monthly mean data.

The governing equations are solved applying a variational Petrov-Galerkin formulation, which includes a stabilizing operator in space and time that improves the classical Galerkin approach. A continuous linear interpolation in space and time is used to approximate the searched solution of the discrete problem.

The eastern pacific ocean domain extends from the equator to 30°S including the more prominent geographical coastline changes. At the open boundaries (sea-side) weakly reflective boundary conditions are used.

The presented results confirm the typical observed mean SST for a generic February month: colder waters along the coastline between the 5°S to 19°S and from the 25° S to the south are generated; in the sector between the 19°S to 25°S, the SST is warmer as compared to those sectors, the intrusion of warm water pattern from the north is also predicted.

These results indicate that the proposed finite element model is able to capture the most relevant hydrothermal dynamical features of this coastal ocean which are in good agreement with the real observed behavior.

Nevertheless, the present paper is still a first step on the modelling of mesoscale circulation. The model is simple and improvements are necessary. Particularly to simulate the complex circulation in the pacific ocean where the superficial and sub-superficial countercurrents are the main modelling challenger.

A next step in the study of the eastern pacific ocean will be the inclusion of another dynamic lower layer (2 ½ layer model). Moreover, countercurrent forcing terms will also be added to the physical model aiming to a more realistic simulation of other typical dynamic features of

Although MSF, MED and RO are nowadays the most conventional techniques used, they present a higher efficiency when connected to a hybrid desalination process, that combines two or more techniques, for example, RO-MSF, RO-MED and RO-VC. As the trend to the use of MSF units is decreasing, installations MSF-RO must be considered promising alternatives.

Table 2. Costs comparison for the state and autonomy service of water and sewer in São Paulo State

	SAAEG		SABESP	
m^3/month	Industrial	Residential	Industrial	Residential
0 - 10	3.94 US$/month	1.73 US$/month	6.88 US$/month	3.43 US$/month
11 - 20	0.68 US$/$m^3$	0.33 US$/$m^3$	0.81 US$/$m^3$	0.48 US$/$m^3$
21 - 50	1.26 US$/$m^3$	0.56 US$/$m^3$	1.32 US$/$m^3$	0.73 US$/$m^3$
More than 50	1.94 US$/$m^3$	0.92 US$/$m^3$	1.55 US$/$m^3$	0.87 US$/$m^3$

Note: (a) conversion factor: 1US$= 2.80 R$ (b) relative values to the price charged by the water offer (c) SAAEG: Autonomy Service of water and sewer of Guaratinguetá (d) SABESP: Basic Sanitation Company of State of São Paulo (2004)
Sources: <http://www.saaeg.com.br/tarifas.htm> and <http://www2.sabesp.com.br/agencia/informese/tarifas.pdf >, access in 16/04/2004

In special conditions, reverse osmosis process is increasingly cited as the recommended choice, mainly when increases in the fuel costs for installations MSF and MED are observed. Hybrid system design, composed by RO/MSF or RO/MED associations, as cited in Van der Bruggen and Vandecasteele (2002) and Altmann (1997), respectively, could become economically feasible, although they are not still commonly operated.

Other hybrid systems can be visualized, as integrated units of seawater management, brackish water and water reuse for human consumption and agriculture, in which a combined cycle of gas turbine/steam turbine is associated with RO and MED installations, according to Uche, Serra and Valero (2001).

Table 3. Typical range of desalinated water cost

Components	Contribution, %
Capital recuperation cost	30 – 50
Energetic cost	30 – 50
Operation and maintenance	15 – 30

REVIEW OF THE INTERNATIONAL EXPERIENCE

MSF desalination technology is used for more than 50 years in Arab countries as a result of its strong restrictions of drinking waters availability, as described by El-Nashar (2001).

Bahrain, Oman, Qatar, Saudi Arabia, United Emirates Arab and Kuwait pertain to a region with severe lack of renewed water resources, and in the last country more than 95% of the drinking water is produced from desalination, as described for Azoury (2001).

The desalination capacity of such Gulf countries and the corresponding percentages of use of each desalination process, according to Azoury (2001), are summarized in Tab. 4.

Table 4. Desalination capacities in the Gulf

Country	Capacity ($10^6 m^3$/y)	MSF (%)	MED (%)	VC (%)	RO (%)	ED (%)
Bahrain	113	52.02	0.00	1.46	41.73	4.50
Kuwait	562	95.47	0.68	0.00	3.39	0.33
Oman	70	84.06	2.18	0.00	11.73	0.00
Qatar	207	94.43	0.64	3.26	0.00	0.00
Saudi Arabia	1917	65.66	0.31	1.21	30.97	1.85
U.A.E.	790	89.80	0.38	2.97	6.49	0.24

Uche, Serra and Valero (2001) present a desalination alternative to the Spanish Hydrological Plan that initially foresaw the transposition of Elbro river course. The alternative is based on a combined desalination cogeneration system to reverse the fresh water scarcity in littoral areas that occurs due to the extreme increase of the tourism associated with an intense agriculture in half-barren regions. The authors consider the use of desalination by RO-MED hybrid process in association to a combined cycle cogeneration system.

The cogeneration system investment costs to fulfill electric demand are analyzed, as well as desalinated water investment costs are investigated as a function of the installation size. Another analysis done by these authors consisted of seawater and brackish water desalination by reverse osmosis for drinking water production, integrated to a unit of residual water treatment, which would supply water for irrigation, as showed by Fig. 5.

Although the hybrid unit depends on the designed capacity and on electricity and fuel prices, they offer more attractive returns compared to the Elbro river transposition process alternative. This model may be an interesting alternative to be thought for the Brazilian northeast region, in which water scarcity is a problem in the major part of the States.

Al-Mutaz (1996) presents a comparative analysis between MSF and RO units in a historical and worldwide context, but the study is focused on the Saudi Arabia regions, showing the configurations in operation, the cities where they are located, the installed capacity and some aspects of chemical

eastern oceans related to their sub-superficial dynamics and their interaction with the surface layer.

ACKNOWLEDGEMENT

This research was partially supported by CNPq, FAPERJ/PRONEX 2003 nº E26/171.199/2003 and MCT/PCI.

REFERENCES

Almeida R. C., Galeão A. C., Silva R.S., 1986. "Adaptive Methods for the Compressible Euler and Navier-Stokes Equations", Finite Elements in Fluids , 2, 337-346, Barcelona.

Bova, S.,W., Carey G.,F., 1995. "An Entropy Variable Formulation and Petrov-Galerkin Methods for the Shallow Water Equations". In G. Carey, John Wiley, LondonEngland, Finite Element Modeling of Environmental Problems-Surface and Subsurface Flow and Transport, 85-114.

Brooks A.N., Hughes T. J. 1982. "Streamline Upwind Petrov-Galerkin Formulations for Convection-Dominated Flows with Particular Emphasis on the Incompressible Navier-Stokes Equations", Comput. Meths. Appl. Mech. Engrg. 32, 199-259.

Carbonel, C., Galeão, A. C. N. R., 2004. A Space-Time Petrov-Galerkin Model of the Upper Coastal Ocean Hydrodynamics in Limited Area Domain. Relatorio de Pesquisa e Desenvolvimento do LNCC, 10/2004.; ISSN 0101.6113.

Carbonel C. 2003. Modelling of Upwelling-Downwelling Cycles Caused by Variable Wind in a Very Sensitive Coastal System. Continental Shelf Research, 23(16), 1559-1578.

Carbonel C., Galeão A.C., Loula A., 2000. "Numerical Study of Petrov-Galerkin Formulations for the Shallow Water Wave Equations". Journal of the Brazilian Society of Mechanical Sciences, Vol. XXII,No 2, 231-247.

Da Silva , A. M. M., Young C.C., Levitus S., 1994. NOAA Atlas NESDIS 6. U.S. Department of Commerce , NOAA, NESDIS.

Fofonoff N. P., 1962. Dynamics of Ocean Currents. In: The Sea, Ed. M.N. Hill, New York, Vol 1, 323p.

Hantel M., 1971. Zum Einfluss des Entrainmentprozesses auf the Dynamik der Oberflachenschicht in einem tropisch-subtropischen Ozean. Deutsche Hydrographische Zeitschrift. Jahrgang 24, 1971, Heft 3.

Iskandarani, M., Haidvogel, D.B., Boyd, J.P., 1995. A Staggered Spectral Model with Application to the Oceanic Shallow Water Equations. Int. J. Numer. Meth. Fluids 20, 393414.

Mendelssohn, R., Schwing F.B., 2002. Common and uncommon trends in SST and wind stress in the California and Peru-Chile current systems. Progress in Oceanography , 53, 141162.

Lluch-Belda, D., Schwartzlose, R. A., Serra, R., Parrish, R., Kawasaki, T., Hedgecock, D., & Crawford, R. J. M.,1992. Sardine and anchovy regime fluctuations of abundance in four regions of the world oceans: a workshop report. Fisheries Oceanography, 1, 339347.

O'Brien J., Heburn G.W., Peffley M., Preller R., Thompson J.D., 1979. Peru Upwelling Models. Depts. of Meteorology and Oceanography, Florida State University, Tallahasse.

Parrish, R. H., Bakun, A., Husby, D. M., & Nelson, C. S., 1983. Comparative Climatology of Selected Environmental Processes in Relation to Eastern Boundary Current Fish Production. FAO Fisheries Report, 291, 731778.

Preller, R., O'Brien, J.J., 1980. The Influence Of Bottom Topography on Upwelling of Peru. Journal of Physical Oceanography 10, 1377-1398.

Ribeiro F.L.B.,Galeão A.C., Landau L. A Space-Time Finite Element Formulation for Shallow Water Equations. In: Development and Application of computer Techniques to Environmental Studies VI. Comp. Mechanics Publications, 1996,403-414.

Rosenfeld L.K., Schwing F.B., Garfield N., Tracy D.E., 1994. Bifurcated flow from na upwelling Center: a Cold Water Source for Monterey Bay. Continental Shelf Research, 14(9), 931-964.

Shakib F. , 1988. "Finite Element Analysis of the Compressible Euler and Navier Stokes Equations". Phd. Thesis, Stanford University.

Yoshida Kozo, 1967. Circulation in the Eastern Tropical Ocean with Special References to Upwelling and Undercurrents. Japan Journal of Geophysics, 4(2), 1-75.